ENGINEERING TRANSACTIONS • *Engng. Trans.* • **53**, 2, 119–131, 2005
Polish Academy of Sciences • Institute of Fundamental Technological Research
10.24423/engtrans.435.2005

ALGORITHMS OF THE METHOD OF STATICALLY ADMISSIBLE DISCONTINUOUS STRESS FIELDS (SADSF) – PART IV

W. Bodaszewski

Kielce University of Technology
Tysiąclecia P.P. 7, 24-314, Poland
e-mail: wboda@tu.kielce.pl

Summary of the whole paper: By now, the SADSF method is practically the only tool of shape design of complex machine elements that provides an effective solution, even to the problems of 3D distribution of the material, and at the same time it is still enough user-friendly to be useful for engineers. This unique property of the method is due to the existence of its simple applicatory version. When using it, a design engineer does not need to solve by oneself any statically admissible field – which could be very difficult – but obtains such a solution by assembling various ready-made particular solutions. The latter are in general obtained by means of individual and complex analyses and provided to a designer in a form of libraries.

The algorithms presented in this paper break up with the individual approach to a particular field. The algorithms are the first ones of general character, as they apply to the fundamental problems of the method. The algorithms enable solving practically any boundary problem that one encounters in constructing 2D statically admissible, discontinuous stress fields, first of all the limit fields. In the presented approach, one deals first with the fields arising around isolated nodes of stress discontinuity lines (Parts II and III), then integrates these fields into 2D complex fields (Part IV).

The software, created on the basis of the algorithms, among other things, allows one to find quickly all the existing solutions of the discontinuity line systems and present them in a graphical form. It gives the possibility of analysing, updating and correcting these systems. In this way, it overcomes the greatest difficulty of the SADSF method following from the fact that the systems of discontinuity lines are not known a priori, and appropriate relationships are not known either, so that they could be found only in an arduous way by postulating the line systems and verifying them.

Applicatory version of the SADSF method is not described in this paper; however, a reference is given to inform the reader where it can be found.

PART IV

INEGRATION OF FIELDS AROUND NODES INTO PLANAR COMPLEX FIELDS

Summary of Part IV: In this part of the paper, the author presents a general concept of algorithms of two program modules that integrate component fields around nodes into planar complex fields. The first module, the auxiliary one called module $\mathbb{C}$, is used to construct the objects of incidence of the regions and the lines that are generated automatically, based on

a freehand sketch of the field structure – which can be drawn, for example, on the monitor screen by means of a mouse. The proper integration, however, is performed by the second module, called module $\mathbb{B}$, which utilises both the incidences brought in by module $\mathbb{C}$, and the solutions of component systems of stress discontinuity lines around nodes – the latter obtained using the module called $\mathbb{A}$. The individual partial problems are still demonstrated here, and the example of the already known solution of the field type $f90$ is used for this purpose.

Attention is also focussed on the effects of partial autonomy that are revealed in the integration problems. These effects consist in decoupling of two systems of conditions: the one defined on geometrical parameters, and that based on stress parameters. The conditions are utilised, for example, in the algorithms of the application version software for finding particularly complicated fields that could contain as much as several dozens of homogeneous regions. An example of such a solution is shown along with its application to shaping complex elements of a structure. The example confirms once again great potential of the SADSF method.

Key words: shape design, limit analysis, numerical methods.

15. Planar complex fields

15.1. Parametric description of field

Let us consider an uncomplicated, planar stress fields (see Figs. 1 and 19d), in which stress discontinuity lines form planar networks consisting of segments of a straight line, and assume that the state of stress in each mesh of the network is homogeneous. On the physical plane these fields are defined by the set $\{\boldsymbol{\sigma}, \mathbf{a}, \mathbf{D}\}$ (1.1).

If we assume – as in previous parts of the work – that the fundamental component units of complex fields are the fields around their nodes, we recognise the complex field as the one created of at least two fields around nodes. In the case when we consider limit fields and apply yield conditions in the parametrised form (6.2), the set (1.1) – describing the complex field – can be expressed in a more convenient form:

$$\{\boldsymbol{\omega}, \boldsymbol{\phi}, \mathbf{a}, \mathbf{D}\}, \tag{15.1}$$

where: $\boldsymbol{\omega} \equiv \{\overset{(\alpha)}{\omega}\colon\ \alpha = 1..T\}$, $\boldsymbol{\phi} \equiv \{\overset{(\alpha)}{\phi}\colon\ \alpha{=}1..T\}$, $\mathbf{a} \equiv \{\overset{(w)}{a}\colon\ w = 1..W\}$.

In this part of the work we still assume the Huber–Misses condition as the preferable one. However, this will be explicitly visible only in the example illustrating the features of the integrating algorithms. Although the algorithms themselves are based on procedures that depend on yield conditions, these procedures are used only as auxiliary means, namely to recreate complete sets of data out of the irreducible sets provided by the module $\mathbb{A}$.

15.2. Structural objects

The structural objects can be created in many ways, depending on specificity of the problems or particular applications. In the case of networks of substantially irregular stress discontinuity lines, it is convenient to transform them first into structurally homogeneous systems. This can be done, for example, by dividing polygonal meshes into triangular ones by introducing additional segments of the lines that are no longer the stress discontinuity lines. The object **D** can then be defined in the form of a rectangular matrix of dimensions $T \times 3$, whose rows specify numbers of nodes associated with the vertices of consecutive triangular regions α ($\alpha = 1..T$), ordered in a uniform way for the whole network.

For the field of Fig. 19d with application of the convention of numbering the nodes and triangles assumed there, the matrix representing the object **D** has the form shown directly below the sketch of the field structure depicted in Fig. 19d. Because the homogeneous regions bounded by the broken lines between the vertices (1,5,6,7) and (2,8,4,3) are quadrilaterals (see Fig. 19c), we have introduced additional segments {6,7}, {8,3}. In order to emphasise that these are not stress discontinuity lines, the two segments are drawn as broken lines in Fig. 19d.

One of important reasons for defining the structural objects **D** in this particular way is the fact that it can be mapped onto other necessary structural objects. Among those there is one, denoted in the algorithms by an illustrative three-letter symbol IST, whose example form is shown under the graph 19b. This form, as well as the object **D**, are both valid for the field of Fig. 19. As it can be seen, the object has the form of a matrix of dimensions $L \times 2$, whose rows are associated with the numbers of segments of stress discontinuity lines ($1..L$) and contain specification of numbers of the homogeneous regions α_1, α_2 adjacent to these lines (this explains the use of **ST** in object's denotation). Then, the object **IST** comprises the information allowing for setting the systems of conditions on individual stress discontinuity lines. This property has been already exploited in algorithmic creation of systems of equations and inequalities ([4]) based on the general recursive formulas presented in Part II of this work.

The object **IST** is a derivative one with respect to object **D**, as it is obtained in the result of the unique mapping $\mathbf{D} \rightarrow \mathbf{IST}$. The further structural objects, defined for the purposes of the algorithm of integration of fields around the nodes, which could be derivatives of **D** or not, will be consequently introduced in the following sections. An illustrative denotation $\mathbf{ITN} \equiv \mathbf{D}$ (triangles-nodes) will also be used there as a rightful equivalent of **D**. Then, the two symbols under the graph in Fig. 19b are identical.

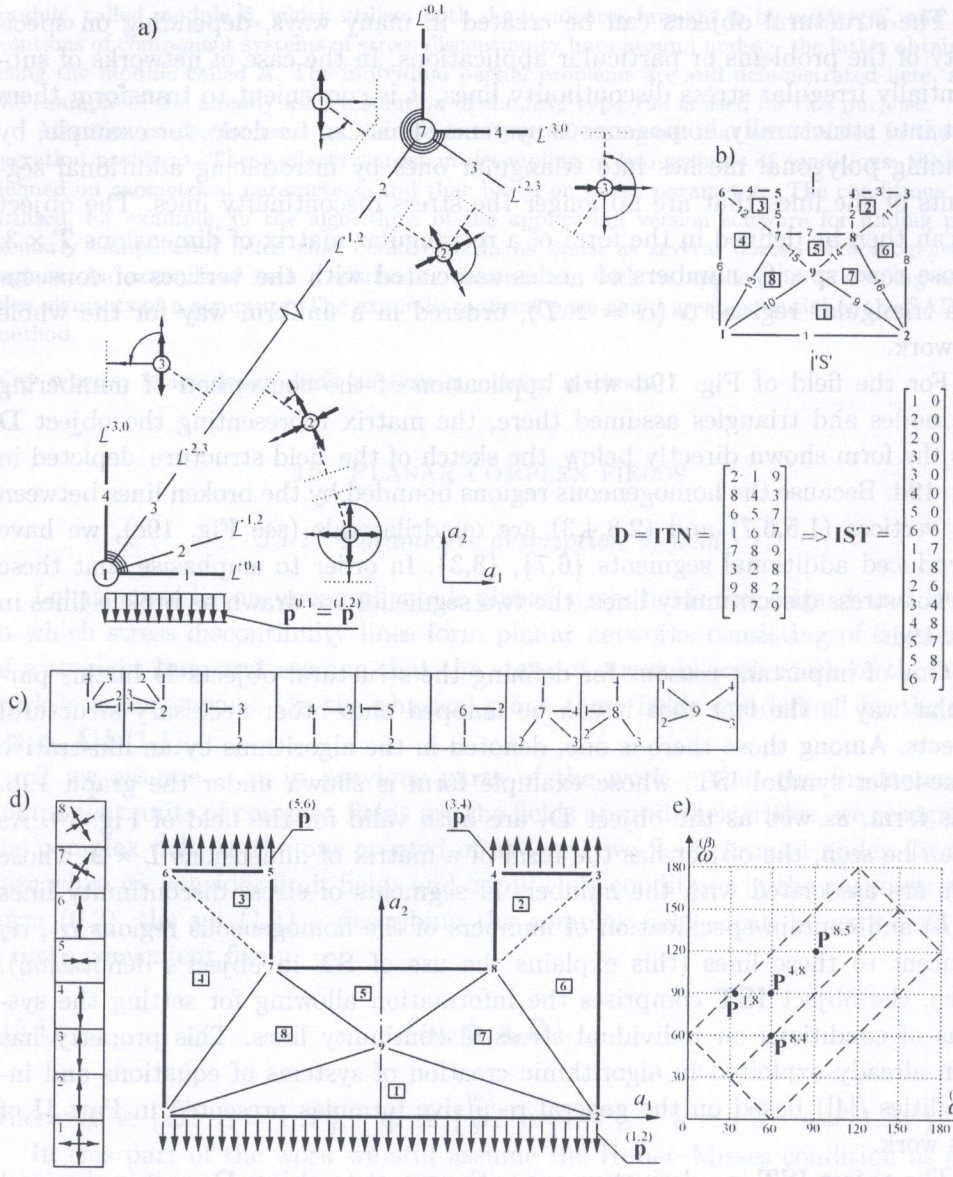

FIG. 19. Field type $f90$ solved for the Huber–Mises yield condition with the data: $\{\overset{(1,2)}{\mathbf{p}} = [\,0.0000, -0.8369]\cdot k,\ \overset{(3,4)}{\mathbf{p}} = [0.0000, 1.7321]\cdot k,\ \overset{(5,6)}{\mathbf{p}} = [0.0000, 1.7321]\cdot k\ \overset{(1)}{\mathbf{a}} = (-80,0),\ \overset{(2)}{\mathbf{a}} = (80,0),\ \overset{(3)}{\mathbf{a}} = (80,90),\ \overset{(6)}{\mathbf{a}} = (-80,90)\ [\mathrm{mm}]\}$, $k = \sigma_{\mathrm{pl}}/\sqrt{3}$; a) limit fields around nodes 1 and 7; b) sketch of the initially assumed structure and the objects **D** and **IST** consistent with the structure; c) limit structures of stress discontinuity lines around all nodes of the field; d) complex field; e) set of images $\mathbf{P}^{\alpha,\beta}$ of stress discontinuity lines in area Λ.

15.3. The conditions of structure preservation

The essential feature of the object **D** defined in this way is the simplicity of the conditions, formulated on the basis of this object, that are used to verify the existence of the place for realisation of each homogeneous region on the plane $\{a\}$. In order to do so, it is enough to demand for the fulfilment of the straightforward conditions (1.7), presented in Part I, for all the triangles that make up the field.

The mentioned conditions (1.7) are called the geometrical conditions of preservation of the structure of stress discontinuity line system. The equivalent conditions, formulated at the stage of fields around nodes, were the inequalities (10.1). They express a similar demand, but there it is expressed in the form of weaker conditions, which allow for the angles between the consecutive discontinuity lines being greater than π. One has also neglected introducing the artificial division lines there, and the homogeneous regions have the form of half-infinite circular segments.

Obviously, the structure of the stress discontinuity line system is preserved if there exists each of the originally established homogeneous regions and each line $\mathcal{L}$, and if the condition (9.3), called the static condition of existence, is satisfied for every line.

16. Integration of fields around nodes into planar complex fields

16.1. Example of analysis of component fields around nodes of field type f90 (Fig. 19)

Let us consider an example of uncomplicated and generally known field type $f90$ previously shown in Fig. 1. The example will be used to illustrate the concept of solving planar complex fields that consists in analysing first the fields around individual nodes, and then integrating them into more complicated systems. The example will be presented as an illustrative drawing, and at this stage the integrating algorithms will not be used. The procedure described in the example, formulated in a more precise form, is also used in the mentioned algorithms as well as in the latest application versions ([3, 5]).

It is necessary to find only two fields around the nodes in order to solve the field. To avoid repetition of the already known results, let us assume that one of the fields is a variant of field type B. It is shown in Fig. 16, and is also presented in Fig. 19a after being completed with the lines $\mathcal{L}^{0,1}$, $\mathcal{L}^{3,0}$ separating the external regions from the stress-free areas. Similarly as in Figs. 19b, d, the considered node will be denoted by number 7, and the other node by number 1.

To help one imagining the location of the two nodes in the complex field, in Fig. 19 we present a sketch of the initially assumed structure of a field type $f90$.

Such a sketch, drawn 'manually' with a mouse on the monitor screen, is the starting point for solving any complex field. The numbers assigned to individual nodes and homogeneous regions establish the system of their mutual associations recorded in the structural object $\mathbf{D} \equiv \mathbf{ITN}$.

It is visible in Fig. 19b that the coupling between the fields around nodes 1 and 7 (Fig. 19a) is realised in such a way that the homogeneous region 3 of the field around node 1, and the region 1 around node 7 constitute, in this complex field, the same triangular homogeneous region denoted by 4 in Fig. 19b.

Similarly, the homogeneous regions 2 around nodes 7 and 1 constitute the region 8 in the complex field (Fig. 19b). The states of stress in the regions around the mentioned nodes must then be identical. In effect, the direction of line $\mathcal{L}^{1,2}$ of the field around node 7, and that of line $\mathcal{L}^{2,3}$ of the field around node 1 are the same. Similarly, the line $\mathcal{L}^{0,1}$ of the field around node 7 is parallel to the line $\mathcal{L}^{3,0}$ of the field around 1 (Fig. 19a). The line $\mathcal{L}^{0,1}$ of field 1, drawn parallel to $\mathcal{L}^{3,0}$ of field 7, is externally loaded with a stress $\mathbf{p}^{0,1}$ whose vector is normal to this line, and whose magnitude is not yet known, as the solution of field around node 7 has been assumed *a priori* (when one uses the numbering convention accepted for the complex field of Fig. 19d, the stress vector would be denoted $\overset{(1,2)}{\mathbf{p}}$).

In the field around node 1 we have:

$$\overset{(3)}{\omega} = 60.00, \quad \overset{(3)}{\phi} = 90.00000°,$$
$$\overset{(2)}{\omega} = 90.00, \quad \overset{(2)}{\phi} = 117.36781°,$$
$$\overset{(1)}{\phi} = 0 \quad \text{or} \quad \overset{(1)}{\phi} = 90°,$$

where $\overset{(\alpha)}{\phi}$ are measured in the system $\{a\}$, where the complex field has been defined.

In order to ensure the existence of a physical place for the region 8 (Fig. 19b,d), one has to demand that the versor of line $\mathcal{L}^{1,2}$ be contained between the versors of lines $\mathcal{L}^{0,1}$ and $\mathcal{L}^{2,3}$. The state of stress in the region 1 of this field, namely the parameter $\overset{(1)}{\omega}$, is not yet known, and it must be determined. In order to do so, for $Q^{1,2} = 1, 2$, we formulate two equations of type (7.1) in the form:

(a) $$\Delta\phi\left(\overset{(1)}{\omega}, \overset{(2)}{\omega}, Q^{1,2}\right) = \overset{(2)}{\phi} - \overset{(1)}{\phi},$$

into which we substitute $\overset{(1)}{\phi} = 0°$, or $\overset{(1)}{\phi} = 90°$. Due to the conventions concerning the system $\{\xi\}^{(0)}$, it is more convenient to assume $\overset{(1)}{\phi} = 180°$ instead of $\overset{(1)}{\phi} = 0°$, which does not change the result on the physical plane. We then substitute (see Table 1):

$$\overset{(2)}{\omega} = 90.00, \quad \overset{(2)}{\phi} - \overset{(1)}{\phi} = -62.6322° \quad \text{or} \quad \overset{(2)}{\phi} - \overset{(1)}{\phi} = 27.36781°$$

Table 1. Parameters of component fields around nodes 1 and 7, and the parameters of complex field type $f90$ of Fig. 19 – solved for the Huber–Mises condition.

– parameters of field arround node 1:

	$\omega[3] = 60.00000$	$\omega[2] = 90.00000$	$\omega[1] = 35.26439$	
	$\sigma_1/k = 1.73205$	$\sigma_1/k = 1.00000$	$\sigma_1/k = 1.99156$	$\sigma_1/k = 0.00000$
$\sigma_1/k = 0.00000$	$\sigma_2/k = 0.00000$	$\sigma_2/k = -1.00000$	$\sigma_2/k = 0.83686$	$\sigma_2/k = 0.00000$
$\sigma_2/k = 0.00000$	$\phi[3] = 90.00000$	$\phi[2] = 117.36781$	$\phi[1] = 180.00000$	$\phi[0] = 180.00000$
$\phi[4] = 90.00000$	$\Delta\nu[3] = 35.26439$	$\Delta\nu[2] = 37.10342$	$\Delta\nu[1] = 17.63219$	$\Delta\phi[0] = 0.00000$
	$\Delta\phi[3] = 0.00000$	$\Delta\phi[2] = -27.36781$	$\Delta\phi[1] = -62.63219$	$\Delta\gamma[0] = 270.00000$
	$\Delta\gamma[3] = 90.00000$	$\Delta\gamma[2] = 27.36781$	$\Delta\gamma[1] = 287.63219$	$q[0] = 3$
	$q[3] = 0$	$q[2] = 1$	$q[1] = 4$	

$\nu[3,0] = 450.0000$	$\nu[2,3] = 414.7356$	$\nu[1,2] = 377.6322$	$\nu[0,1] = 360.0000$ $p[1]/k = 0.0000$ $p[2]/k = 0.8369$

4	3	2	1	0
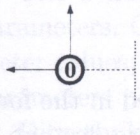		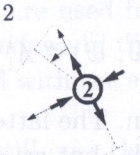	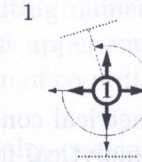	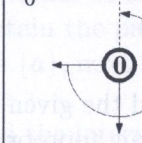

– parameters of field arround node 7:

	$\omega[3] = 120.00000$	$\omega[2] = 90.00000$	$\omega[1] = 60.00000$	
	$\sigma_1/k = 0.00000$	$\sigma_1/k = 1.00000$	$\sigma_1/k = 1.73205$	$\sigma_1/k = 0.00000$
$\sigma_1/k = 0.00000$	$\sigma_2/k = -1.73205$	$\sigma_2/k = -1.00000$	$\sigma_2/k = 0.00000$	$\sigma_2/k = 0.00000$
$\sigma_2/k = 0.00000$	$\phi[3] = -90.00000$	$\phi[2] = -62.632190$	$\phi[2] = -90.00000$	$\phi[0] = -90.00000$
$\phi[4] = 0.00000$	$\Delta\nu[3] = 35.26439$	$\Delta\nu[2] = 90.00000$	$\Delta\nu[1] = 144.73561$	$\Delta\phi[0] = 0.00000$
	$\Delta\phi[3] = 90.00000$	$\Delta\phi[2] = -27.36781$	$\Delta\phi[1] = 27.36781$	$\Delta\gamma[0] = 270.00000$
	$\Delta\gamma[3] = 180.00000$	$\Delta\gamma[2] = 117.36781$	$\Delta\gamma[1] = 54.73561$	$q[0] = 3$
	$q[3] = 0$	$q[2] = 2$	$q[1] = 1$	

$\nu[3,0] = 360.0000$	$\nu[2,3] = 324.7356$	$\nu[1,2] = 234.7356$	$\nu[0,1] = 90.0000$

4	3	2	1	0
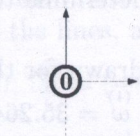	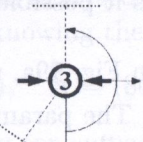	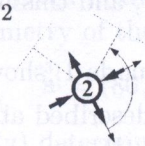	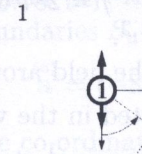	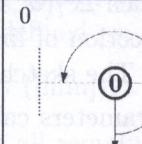

– σ, a, D:

α	D	σ_{11}/k	σ_{22}/k	σ_{12}/k	σ_{eq}/σ_{pl}	ω	ϕ
1	2 1 9	1.992	1.837	0.000	1.000	35.2644	−180.0000
2	8 4 3	0.000	1.732	0.000	1.000	60.0000	90.0000
3	6 5 7	0.000	1.732	0.000	1.000	60.0000	−90.0000
4	1 6 7	0.000	1.732	0.000	1.000	60.0000	90.0000
5	7 8 9	−1.732	0.000	0.000	1.000	120.0000	−90.0000
6	3 2 8	0.000	1.732	0.000	1.000	60.0000	−90.0000
7	9 8 2	−0.577	0.577	0.816	1.000	90.0000	242.6322
8	1 7 9	−0.577	0.577	−0.816	1.000	90.0000	117.3678

w	a_1	a_2
1	−80.0000	0.0000
2	80.0000	0.0000
3	80.0000	90.000
4	41.347	90.000
5	−41.347	90.000
6	−80.0000	90.000
7	−41.347	54.664
8	41.347	54.664
9	0.000	25.427

Table 1. [cont.]

INL =

l_1	l_2	l_3	l_4	l_5	l_6	l_7	w
1	4	3	2	0	0	0	1
1	4	2	3	0	0	0	2
1	2	0	0	0	0	0	3
1	2	0	0	0	0	0	4
1	2	0	0	0	0	0	5
2	1	0	0	0	0	0	6
1	4	0	2	3	0	0	7
1	4	2	0	3	0	0	8
1	4	3	2	0	0	0	9

INN =

w_1	w_2	w_3	w_4	w_5	w_6	w_7	w
2	6	7	9	0	0	0	1
3	1	8	9	0	0	0	2
4	2	8	0	0	0	0	3
8	3	0	0	0	0	0	4
6	7	0	0	0	0	0	5
5	1	7	0	0	0	0	6
5	8	6	1	9	0	0	7
7	4	9	3	2	0	0	8
7	8	2	1	0	0	0	9

Equations (a) must be solved with the condition:

(b) $$(\overset{(1)}{\omega}, \overset{(2)}{\omega}) \in \Lambda^{1,2}_{1,2}$$

and the given geometrical condition. The latter should be expressed in the form of an appropriate analytical formula, but we omit explaining how to do that.

It is evident that the problem formulated in such a way is exactly equivalent to the case of the elementary problem <**3**> described in Sec. 13.

We obtain here four roots: $\overset{(1)}{\omega}$= 144.7356, 120.0000, 60.0000, 35.2644. Substituting them into formulae (7.1), we can calculate $\Delta\phi(\overset{(1)}{\omega},\overset{(2)}{\omega},Q^{1,2})$ for all parameters of the families $Q^{1,2} = 1, 2$, and then verify the fulfilment of conditions (a) and the geometrical limitations imposed on the field of versors of line $\mathcal{L}^{1,2}$. The whole set of these conditions is satisfied for $\overset{(1)}{\omega} = 35.2644$ and $q^{1,2} = 4$, for which $\Delta\gamma(\overset{(1)}{\omega}, \overset{(2)}{\omega}, q^{1,2}) = 287.6322°$, and this makes it possible to determine the direction of line $\mathcal{L}^{1,2}$.

The sketch of the field around node 1, shown in Fig. 19a, was drawn for the parameters calculated in the way described above. The parameter $\overset{(1)}{\omega} = 35.2644$ is related to the principal stresses $\overset{(1)}{\sigma}_1 = 1.9916\,k$, $\overset{(1)}{\sigma}_2 = 0.8369\,k$, so that the components of the stress vector applied to line $\mathcal{L}^{0,1}$ ($\mathbf{n} = (0, -1)$), given in the system $\{a\}$, are equal to: $p_2^{0,1} = -0.8369\,k$, $p_1^{0,1} = 0$.

Table 1 juxtaposes the numerical results and the sketches of the states of stress in the homogeneous regions of fields around the component nodes 1 and 7. It facilitates a more precise apprehension of the numerical data associated with the presented solution, including the possibility of searching for intermediate values of individual variables. The data are shown in the form consistent with that edited on the monitor screen during the session with module $\mathbb{A}$

The states of stress in individual homogeneous regions and their parameters are presented in separate windows, mutually interrelated. In the pictures, we

have applied the following method of graphical presentation:

- bold arrows denote principal stresses $\overset{(\alpha)}{\sigma}_1$, $\overset{(\alpha)}{\sigma}_2$; the axis $\{\xi_1\}^{(\alpha)}$ has the direction $\overset{(\alpha)}{\sigma}_1$;
- the numbers of homogeneous regions α are circumscribed with circles; the centres of these circles are located at the points (0,0) of the local systems $\{\xi\}^{(\alpha)}$;
- the angles $\Delta\gamma(\overset{(\alpha)}{\omega}, \overset{(\alpha+1)}{\omega}, q^{(\alpha,\alpha+1)})$ are marked by arches ended with arrows;
- the angles $\Delta\phi(\overset{(\alpha)}{\omega}, \overset{(\alpha+1)}{\omega}, q^{(\alpha,\alpha+1)})$ have no special denotations, as they can be easily identified based on the positions of individual local systems $\{\xi\}^{(\alpha)}$;
- the discontinuity lines $\mathcal{L}^{\alpha,\alpha+1}$ separating regions α, $\alpha+1$ are drawn as dotted lines, while the lines perpendicular to them are dashed lines.

The windows over the graphs are used for editing numerical values of field parameters. Consequently, the windows in the first upper row contain the parameter values; first these associated with the system of co-ordinates $\{a\}$, next the parameters pertaining to $\{\xi\}^{(\alpha)}$.

Directly below that row, but still over the graphs, one can find the intermediate windows, whose positions are selected to illustrate their references to the states of stress in both adjacent regions. There are given the values of parameters $\nu^{\alpha,\alpha+1}$ and the applied external loads $\mathbf{p}^{\alpha,\alpha+1}$ if these take non-zero values. The components of these loads are expressed in the systems associated with the lines $\mathcal{L}^{\alpha,\alpha+1}$. It must be emphasised that the system $\{\xi\}^{(0)}$ is defined in a different way than the other ones (see Figs. 4 and 6). Its axis ξ_1 is directed towards the node of line $\mathcal{L}^{0,1}$, while in the other cases the direction is opposite.

Figure 19c depicts the whole set of stress discontinuity lines systems around all the nodes of the analysed field given in the system $\{a\}$. Having the direction of the lines, and knowing the geometry of the boundaries S_u, S_p defined as:

(c) $\overset{(1)}{\mathbf{a}} = (-80, 0)$, $\overset{(2)}{\mathbf{a}} = (80, 0)$, $\overset{(3)}{\mathbf{a}} = (80, 90)$, $\overset{(6)}{\mathbf{a}} = (-80, 90)$ ([mm]),

we can graphically (or numerically) determine the co-ordinates of all remaining nodes.We can also assign the states of stress calculated by means of the module $\mathbb{A}$ to the homogeneous regions of the complex field. In the case when the operations are to be performed by the algorithm, they must be defined on data structures acceptable for the compiler.

16.2. Incidences of regions and lines

The module $\mathbb{C}$ is used to graphically construct the structural objects of stress discontinuity line networks: **ITN**, **IST, ISN**, **INN**, **INL**, which respectively pertain to the incidences of the following types: triangle – numbers of its nodes, segment of line $\mathcal{L}$ – the triangles separated it, segment of line $\mathcal{L}$ – its

nodes, node – adjacent nodes, and node – local numbers of lines that originate from the node. The latter are identical with the numbers given to the lines when solving the field with the aid of implementation of the module $\mathbb{A}$ algorithm.

In the presented algorithms, only **ITN** and **INL** can be independent, although the independence of **ITN** from **INL** is revealed only when it refers to the artificially introduced lines.

The session with the implementation of module $\mathbb{C}$ starts from drawing a sketch, by means of a mouse, of segments of the line $\mathcal{L}$ network. In the next step we numerate the nodes and then the triangles. Based on this graphical information, the module automatically generates the objects **ITN** and **INL**. Obviously, all the lines identified there are treated on equal rights, without paying attention to the stress field, which does not allow for finding the lines that separate regions of identical states. Therefore, an additional correction is needed in order to select such lines. It is accepted that these lines are given number 0. By doing so, all other lines are automatically re-numerated. The most important thing is that the numbers of individual lines $\mathcal{L}^{\alpha,\beta}$ must be consistent with those given when solving the component fields around nodes. It can be proven that, once the objects **ITN, INL** are at our disposal, we can uniquely attest the identity of the regions specified by local numeration (associated with a node) with those specified by global numeration (associated with the complex field). At the same time, we can also identify the states of stress and the status of lines that separate them. In effect, when the solutions of the fields around nodes are given, it becomes possible to combine them into a planar complex field determined on the physical plane $\{a\}$.

In the case of field type $f90$ (see Figs. 19c and 19d), the objects **INL** and **INN** take the forms presented in Table 1.

16.3. Construction of complex field

Let the starting point for the problem be the set of parameters: $\{\boldsymbol{\omega}\}_w \equiv \{\overset{(\alpha)}{\omega}: \alpha = 1..N\}_w$, $\{\boldsymbol{\phi}\}_w \equiv \{\overset{(\alpha)}{\phi} : \alpha = 1..N\}_w$, $\{\boldsymbol{\nu}\}_w \equiv \{\nu^{\alpha,\alpha+1}: \alpha = 0..N-1\}_w$ – determined for individual nodes w by means of the module $\mathbb{A}$, and the co-ordinates of the nodes located on $S_u + S_p$. In this example, the set of these co-ordinates has the form given by equalities (c) (Part IV).

On the basis of **ITN** and **INL**, given by module $\mathbb{C}$, one can select the identical homogeneous regions in the fields around nodes and in the complex field. In effect, the states of stress in all triangular regions $\{\overset{(\alpha)}{\omega}, \overset{(\alpha)}{\phi}: \alpha = 1..T\}$ can be determined.

Similarly, on the basis of **INN** and **INL** (**ITN** $\rightarrow$ **INN**) one identifies the angular parameters of lines originating from the nodes. There holds the relation-

ship: $w_s = INN\,[w,i]$, $1 = INL\,[w,i]$, and this means that the number of node w_s – adjacent to node w – is placed in the object **INN** on the same position as the local number of line 1 originating from this node in the object **INL** (see Table 1).

Obviously, when using this relationship, one must make a correction of denotations of the parameters $\nu^{\alpha,\alpha+1}$. Actually, this correction has already been made in the module $\mathbb{A}$, where – besides of the indices α, $\alpha+1$ – the lines are also numerated with successive natural numbers, $l = 1,2,...$ (the same numbers were given in the module $\mathbb{C}$). In order to mark this small change, denotations used for to the parameters: $\{\boldsymbol{\upsilon}\}_w \equiv \{v^1 : l = 1..L\}_w$ are similar, but printed in fonts of slightly different shapes.

Once we have the object **ITN**, the angular parameters of all its lines $\{\boldsymbol{\upsilon}\}_w$ originating from the nodes, and geometrical description of the boundary $S_u + S_p$, we can determine the co-ordinates of nodes as the points of intersection of the lines, starting from the nodes given on the boundary, and then the currently calculated ones. The procedure is repeated until the locations of all the nodes are determined. The fact that calculation of co-ordinates of a particular node is completed is marked in the algorithm by giving the variable $aB^{(w)}$ the value 'TRUE'.

In the case of field type $f90$, with the given locations of nodes 1, 2, 6, 3 (in the algorithm there is: $aB^{(1)} = aB^{(2)} = aB^{(3)} = aB^{(6)} =$ TRUE), the detailed calculations are carried out according to the following scheme:

$$\{1,2\} \to 9, \quad \{1,9\} \to 7, \quad \{2,9\} \to 8, \quad \{3,8\} \to 4, \quad \{6,7\} \to 5.$$

The field determined in such a way is presented in Fig. 19d, while the calculated set of its internal parameters $\{\boldsymbol{\sigma}, \mathbf{a}, \mathbf{D}\}$ is in the middle part of Table 1. The parameters are defined in the system $\{a\}$.

Figure 19e depicts the area Λ with the images of the individual lines of discontinuity of the solved field.

Generally, the above-described tasks are performed within the module $\mathbb{B}$. Because the module makes use of **ITN**, **INL** and $\{\boldsymbol{\omega}\}_w$, $\{\boldsymbol{\phi}\}_w$, $\{\boldsymbol{\upsilon}\}_w$ – it must communicate with the module $\mathbb{C}$, and also with $\mathbb{A}$. The presented numerical results and the graphs have the form almost identical with that edited on the monitor screen.

We omit describing the details of both integrating algorithms. As far as module $\mathbb{A}$ is concerned, the principle of operation is relatively straightforward, and possible difficulties may appear only when one gets to the level of details. The most important difficulty results from the fact that the objects of incidence are defined on the sets of integer numbers, while the criteria of inclusion may be formulated only on the sets of real numbers.

17. Other applications of integrating module algorithm

The elements of the sets $\{\omega\}_w$, $\{\phi\}_w$, $\{\upsilon\}_w$ are stress parameters, unlike the co-ordinates of nodes, which are classified as geometrical parameters of complex fields. As it follows from the presented example, behind this apparently formal classification there are hidden partial autonomies of the component problems. One of the types of these autonomies, related to the stress parameters, was mentioned in Part III. In this part, the problem has been solved in two separate ways, first on the set of stress parameters, then on the set of geometrical parameters.

This effect allows us to construct not only the algorithms, but also the structures of variables it contains that represent the field parameters. These structures make it possible to describe, in a concise form, the cases of very complicated fields consisting of even several dozens of homogeneous regions.

One of the examples of utilisation of such data structures and the algorithms that operate on them is the solution of the field type $s18$ presented in Fig. 20a ([5]).

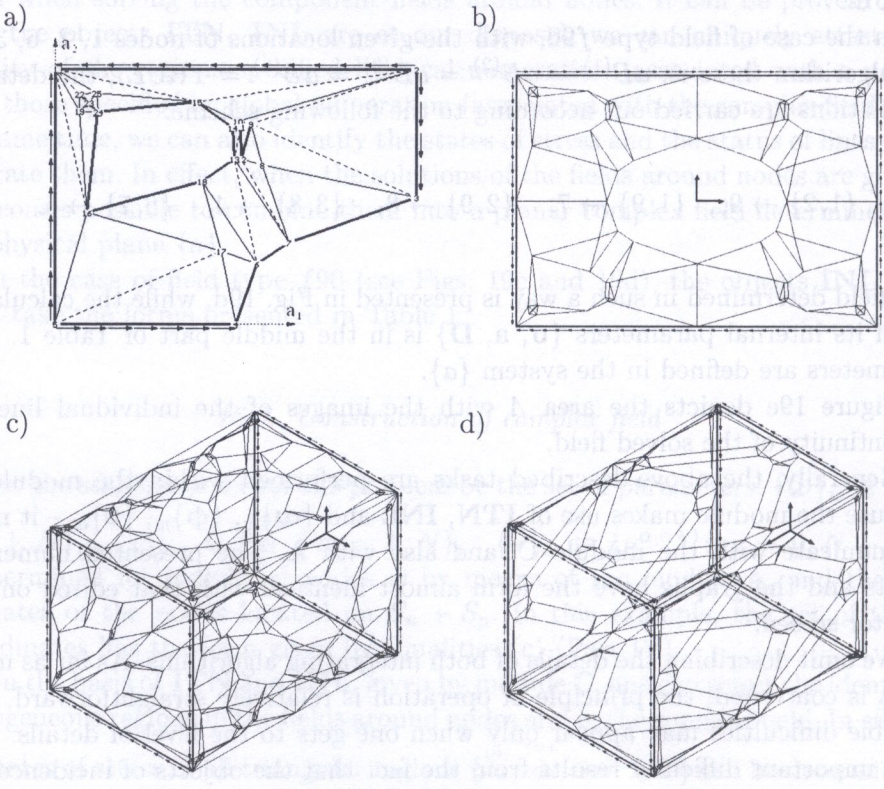

Fig. 20.

The subsequent graphs, Figs. 20b, c, d depict the examples of application of the field, such as: plane elements loaded with shear streses, box sections with holes subjected to torsion and space trusses. Notice that the fields of Figs. 20c and 20d have the same structure, although they are determined for different data.

References

1. W. Szczepiński *Plastic design of machine parts* [in Polish], PWN, Warszawa 1968.
2. W. Bodaszewski *Stress discontinuity line structures in yield zones satisfying the Huber–Mises condition* [in Polish], Engineering Transactions, part 1 **36**, 1, 29–54, 1988, part 2 and 3 **37**, 3, 415–442, 1989.
3. W. Bodaszewski *The software package KNPN for approximated shaping of complex plastic structures*, VIII-th Symposium on Stability of Structures, Łódź University of Technology, Poland, 25–30, 1997.
4. I. Markiewicz *Numerical determination of statically admissible link systems of stress discontinuity lines in limit Huber–Mises's fields* [in Polish], doctoral thesis, Warsaw University of Technology, 1996.
5. Internet website: www.sadsf.net.

Received January 31, 2003.